Pseudomonas aeruginosa orchestrates twitching motility by sequential control of type IV pili movements

Lorenzo Talà[1], Adam Fineberg[2], Philipp Kukura[2], Alexandre Persat[1]*

1. Institute of Bioengineering and Global Health Institute, EPFL, Lausanne, Switzerland
2. Department of Chemistry, Physical and Theoretical Chemistry Laboratory, University of Oxford, Oxford, United Kingdom.

* alexandre.persat@epfl.ch

Prokaryotes have the ability to walk on surfaces using type IV pili (TFP), a motility mechanism known as twitching[1,2]. Molecular motors drive TFP extension and retraction, but whether and how these movements are coordinated is unknown[3]. Here, we reveal how the pathogen *Pseudomonas aeruginosa* coordinates motorized activity of TFP to power efficient surface motility. To do this, we dynamically visualized TFP extension, attachment and retraction events at high resolution in four dimensions using label-free interferometric scattering microscopy (iSCAT)[4]. By measuring TFP dynamics, we found that the retraction motor PilT was sufficient to generate tension and power motility in free solution, while the partner ATPase PilU may only improve retraction in high friction environments. By precisely timing successive attachment and retraction, we show that *P. aeruginosa* engages PilT motors very rapidly and almost only after TFP encounter the surface, suggesting contact sensing. Finally, measurements of TFP dwell times on surface show that tension reinforced the adhesion strength of individual pili to the surface, thereby increasing effective pulling time during retraction. The successive control of TFP extension, attachment, retraction and detachment suggests that sequential control of motility machinery is a conserved strategy for optimized locomotion across domains of life.

Protein filaments decorate the surface of prokaryotes, allowing single cells to physically interact with their surroundings through motility, adhesion, gene exchange and signaling[5,6]. For example, *P. aeruginosa* performs successive rounds of motor-driven TFP extension and retraction to power twitching motility and regulate virulence through mechanosensing[7–9]. Pili retraction motors can generate up to 100 pN, but how such large forces end up powering cell body displacements remains unclear[10,11]. To answer this question, the distribution of individual pili around single cells have been indirectly inferred from tracking of cell body displacements[12]. Also, labeling strategies have largely helped in the visualization of extension and retraction events, but also in deciphering the function of TFP in horizontal gene transfer and mechanosensing[13,14]. These methods are powerful but remain invasive, and are limited by labeling robustness during high-speed or long-term imaging of TFP. As a result, changes in TFP length, number, and extension-retraction frequencies, which ultimately regulate bacterial interaction with the environment, are difficult to measure during

the course of motility. Understanding this connection therefore rests on our ability to visualize and monitor the dynamics of individual TFP on short timescales of extension-retraction (subsecond) and on longer timescales of surface colonization (minutes to hours).

To explore the coordination of their movements, we sought to directly image successive TFP extension-retraction events. iSCAT has previously been used to image single actin filaments *in vitro* without labels[15]. We reasoned that since actin and TFP are both approximately 5 nm-wide protein polymers, iSCAT may enable TFP visualization. To achieve this, we adapted iSCAT to live cell imaging (**Supplementary Figure 1**)[16]. We reduced phototoxicity by using less energetic iSCAT and autofocus laser lines, and reduced unnecessary illumination by adding a shutter in the iSCAT illumination path with a brightfield channel for initial bacteria detection (see **Methods**).

Under brightfield illumination, wild-type (WT) *P. aeruginosa* appeared as rod-shaped without any visible surface structures (**Fig. 1a**). Simultaneous iSCAT images of the same cell revealed micrometer-long extracellular filaments and shorter structures with alternating intensity extending from the cell body (**Fig. 1a**). Cells of in-frame deletion mutants in the pilin subunit gene *pilA* displayed no such slender structures (**Fig. 1b)** suggesting these were TFP. A deletion of the flagellin gene *fliC* removed structures with periodic pattern (**Fig. 1c, Supplementary Figure 2**), suggesting this signal was generated by single helical flagella, which had a periodicity of 1.4 μm ± 0.1 μm (s.e.m., N = 10), consistent with previous measurements for the helical pitch[17]. Quantification of filaments showed that WT had approximately one pilus per cell, *pilA*$^-$ had no TFP, and *fliC*$^-$ had about five (**Fig. 1d**, **Supplementary Figure 2** and **Methods**), and that, as expected, most WT cells had one flagellum and *fliC*$^-$ had zero (**Supplementary Figure 2**).

Live-cell iSCAT can capture multiple successive extension-retraction events while monitoring cell body displacements. For example, **Supplementary Video 1** shows a one minute visualization of a WT cell exhibiting multiple rounds of TFP attachment and retraction. Such sequences allow us to quantify attachment-retraction frequencies while monitoring cell body displacement (**Supplementary Figure 3**). Since the signal generated from the flagellum was stronger than the one from TFP, and that swimming may interfere with twitching motility, we sought to perform most dynamic visualizations in a *fliC*$^-$ background. We tested whether this affected TFP dynamics, and

found that there was no distinguishable differences in cell displacement per retraction and in retraction frequencies between WT and the flagellum-less mutant (**Supplementary Figure 4, Supplementary Video 1 and 2**).

We observed three distinct patterns generated by TFP on iSCAT images: straight dark filaments, straight filaments with alternating black and white contrast, or curved filaments with fainter contrast (**Fig. 2a**). Changes in contrast of a fiber are a manifestation of the shift from constructive to destructive interference with a full phase change corresponding to a spatial shift of $\lambda/2n$, where λ is the illumination wavelength and n the index of refraction of the medium[18]. Intensity values can thus be used as a proxy for in-depth position of TFP[19]. For example, TFP having uniform intensity lay flat against the surface (**Fig. 2a, left panel**). The ones exhibiting successively positive and negative intensity values along their length are at an angle (**Fig. 2a, center and right panels**). As a result, single iSCAT images provide us with the position and orientation of single TFP in three dimensions, thereby allowing to quantitatively infer spatial position on and away from the attachment surface. We could for example observe differences in TFP positioning of standing *vs* horizontal cells[1]. TFP of standing cells, which orient vertically on the surface attached by one pole, were in majority (79%) flat against the surface as in **Fig. 2a**. In contrast, in crawling, horizontal cells, TFP were in most cases (81%) oriented at an angle between the glass surface and the cell pole (**Fig. 1a**). In summary, iSCAT gives us the ability to probe TFP dynamics at high spatial and temporal resolutions in three dimensions, without obstructing native biological functions.

These images highlight two distinct TFP morphologies and dynamics: straight stationary and curved fluctuating filaments. We verified that the straight conformation was a result of tension generated during retraction. At the molecular level, the extension motor PilB polymerizes PilA subunits to drive TFP growth. The two retraction motors PilT and PilU drive retraction by depolymerizing PilA back into the periplasm, but whether their functions are redundant remains unclear[7,20]. *fliC*$^-$ cells had both fluctuating curved and stationary straight TFP (**Fig. 2b**, **Supplementary Video 3**). In contrast, a *pilTU*$^-$ *fliC*$^-$ mutant had only curved TFP that were fluctuating (**Fig. 2c**, **Supplementary Video 4**). This demonstrates that straight TFP are under tension during retraction.

Given the lack of clear function for two retraction motors in *P. aeruginosa*, we sought to identify functional differences between PilT and PilU by visualizing TFP dynamics in respective mutants. Both *pilT* and *pilU* mutants lose their ability to twitch in typical agar stab assay and have been reported as hyperpiliated[21]. In *Neisseria gonorrhoeae*, PilU has no apparent role in twitching motility[22]. In our visualizations, while *pilT*$^-$ *fliC*$^-$ could not retract on the timescales of our visualizations, a *pilU*$^-$ *fliC*$^-$ deletion mutant could still transition to a tensed state, demonstrating its ability to retract TFP (**Fig. 3a, Supplementary Videos 5-6**). In addition, *pilU*$^-$ *fliC*$^-$ tends to have less, not more, TFP compared to *fliC*$^-$, in contrast to *pilT*$^-$ *fliC*$^-$ (**Fig. 3b, Supplementary Videos 5-6**). Thus, cells lacking *pilU* can retract TFP, but still, they do not migrate in typical twitching assays where colonies spread at the interface between a plastic dish and agar (**Supplementary Figure 5**)[20]. We sought to elucidate this paradox by examining TFP dynamic activity. We first found that the length of TFP were identical between *fliC*, *pilU*$^-$ *fliC*$^-$ and *pilT*$^-$ *fliC*$^-$, demonstrating that extension is not affected (**Fig. 3c**). Retraction frequency was slightly decreased in *pilU*$^-$ *fliC*$^-$ compared to *fliC*$^-$ (**Fig. 3d**), which however could not explain a full loss of motility observed in twitching assays. Finally, measurements of displacements in free solution on glass shows that each retraction generates approximately a similar displacement in *fliC*$^-$ and *pilU*$^-$ *fliC*$^-$ (**Fig. 3e, Supplementary Video 2 and 7**). This demonstrated that TFP of cells lacking *pilU* do not lose their ability to generate displacements.

Since dynamics were not grossly affected by the absence of PilU in free solution, we sought to highlight a potential role of PilU in generating retraction force. We visualized twitching motility at the leading edge of colonies sandwiched between glass and agarose surfaces by phase contrast microscopy (we could not implement iSCAT as the gel scatters strongly). We reasoned that the friction between the cell body and the substrate during locomotion in this configuration is higher than in free solution, thereby requiring larger forces to generate displacements during retraction. *fliC*$^-$ cells at the leading edge of expanding twitching colonies were highly motile between glass and a 0.5% agarose gel (**Supplementary Video 8,** top left). In this same configuration, *pilU*$^-$ and *pilU*$^-$ *fliC*$^-$ were barely motile, consistent with twitching assays (**Supplementary Video 8,** bottom). We could recapitulate this defect in *fliC*$^-$ by increasing the friction of the cell body with the surface using higher

agarose concentration, which requires a higher retraction force to generate similar displacement (**Supplementary Video 8,** top right, **Supplementary Figure 6**)**.** Altogether, this suggests that PilU contributes to increasing TFP retraction force in conjunction with PilT, rather than acting as an independent retraction motor. By analogy with the torque-dependent recruitment of flagellar motors, PilU could be activated when PilT reaches a threshold force[23], consistent with the fact that PilU localizes at the leading poles of twitching cells[24]. Alternatively, PilU could regulate PilT activity, for example through direct interaction or by mediating the function of minor pilins inserted in TFP[25]. In summary, *P. aeruginosa* uses one motor, PilT, to twitch in low friction environment, but leverages the companion ATPase PilU to power displacements when friction increases.

A key question arising from these movies of *a priori* random attachment and detachment events is how *P. aeruginosa* orchestrates force generation to drive motility. To optimally generate displacements, cells must coordinate TFP retraction with attachment and detachment (**Fig. 4a**)[3]. Is this sequence actively coordinated or do TFP randomly extend and retract? To answer this, we performed visualizations of each step involved in individual TFP cycles (**Fig. 4b, Supplementary Videos 9 and 10**). We found that the tip of extended TFP occasionally appeared as a stationary dark spot while the remainder of the fiber fluctuated, indicating initial attachment. The same fiber then transitioned to a straight stationary line indicating retraction and tension, before eventually detaching (**Fig. 4c, Supplementary Videos 9 and 10**). We could thus time transitions between attachment, retraction and detachment of single fibers. We first measured the dwell time τ_d defined as the residence time of the pilus on the glass surface from tip attachment to detachment (**Fig. 4a**). The TFP of the retraction-less mutant *pilT*$^-$ *fliC*$^-$ could still attach, with median dwell time of 75 ms [65 - 90 ms] (median and 95% bootstrap confidence interval), which is a measurement of the intrinsic residence time of passive fibers on the surface (**Fig. 4d**). Given that the retraction speed of TFP is about 1 μm.s^{-1}, this would only enable a seemingly short 70 nm displacement per retraction[13]. Surprisingly, the dwell time in cells capable of retraction was, however, much longer: 2,315 ms [1,710 – 2,635 ms] in WT, 997 ms [590 – 1,795 ms] in *fliC*$^-$ and 540 ms [405 – 840 ms] in *pilU*$^-$ *fliC*$^-$ (**Fig. 4a**). This indicates that tension force during retraction enhances TFP adhesion, increasing surface attachment time, thereby improving effective displacements of the cell body. In analogy with

147 the formation of catch-bonds by the adhesin FimH in *Escherichia coli*, tension force may induces a
148 conformational change in the structure of TFP, thereby increasing the strength of its attachment to
149 the surface[26,27]. We also note that dwell times are typically lower than 3 s, thereby allowing TFP
150 release for subsequent extension-retraction cycles, and that *pilU*$^-$ *fliC*$^-$ had slightly decrease dwell,
151 possibly as a consequence of lower retraction strength.

152 The short dwell time of relaxed TFP on the surface suggests that retraction must rapidly take
153 place after attachment. To achieve this, retraction must occur at high frequency or systematically
154 after pilus contact with the surface. The first scenario would lead to inefficient conversion of force
155 into displacement, while the second suggests cells sense contact of their TFP. To identify the
156 strategy *P. aeruginosa* uses to coordinate TFP retraction with attachment; we directly measured
157 tension time τ_t defined as the delay between tip attachment and pilus tension (**Fig.4a**). We found
158 that TFP became tensed 130 ms [95 - 215 ms] after tip attachment in WT and 135 ms [105 – 198
159 ms] in *fliC*$^-$, which was close to the dwell time of relaxed TFP on the surface of *pilT*$^-$ *fliC*$^-$. Also, *pilU*$^-$
160 *fliC*$^-$ had a similar reactivity (τ_t = 150 ms [90 - 155 ms]) (**Fig. 4d**), showing that PilT motors engage
161 rapidly, optimizing retraction efficiency and subsequently increasing the dwell time of TFP on
162 surfaces. This result also hints to the possibility that cells sense tip attachment to rapidly initiate
163 retraction. Measuring the proportion of TFP retraction without attachment further supports this
164 hypothesis: most extended TFP did not retract during the course of visualization unless their tip
165 attached to the surface (**Fig. 4e, Supplementary Figure 7**). This demonstrates that TFP
166 attachment stimulates retraction, and that motors respond to a signal generated by contact of the tip
167 with the surface. Thus, *P. aeruginosa* uses a high-efficiency sensing strategy to deploy and
168 coordinate TFP rather than relying on random motor activation.

169 Our measurements indicate that *P. aeruginosa* precisely coordinates TFP motorized activity with
170 attachment by successively sensing surface contact, initiating retraction by a first motor, improving
171 surface attachment during retraction through a catch bond, and triggering a second motor to
172 generate displacement under high load (**Fig. 4f**). In a same manner as animal locomotion, the
173 sequential control of pili movements could be coupled with sensory feedback enabling
174 transformation into cell displacements, thereby increasing the efficiency of conversion of chemical

energy into mechanical work. For example, animals use multiple sensory inputs such as mechanosensation and proprioception to control and synchronize limb motion during locomotion[28,29]. Here, we suspect that tip contact generates a mechanical signal read out by sensory components that trigger TFP retraction by PilT, and subsequent activation of PilU during twitching under high load. Combining visualizations of bacterial surface structures dynamics with molecular characterizations will eventually generate a holistic understanding of their functions, ultimately helping us understand how microbes physically interact with their environment and highlighting shared strategies among seemingly distant living organisms[30].

Methods

Bacterial strains

Strains and plasmids used in this work were described previously[20]. Double deletion mutant *pilTU*$^{-}$ *fliC*$^{-}$ was generated by conjugation of *pilTU*$^{-}$ mutants with the plasmid pJB215 using a standard mating protocol[31].

Glass coverslip preparation

Glass coverslip (Marienfeld, 22x40 mm No 1.5) were cleaned as described in Young et al.[32]. Briefly, they were washed sequentially with distilled water, ethanol, distilled water, isopropanol, distilled water, ethanol, distilled water and excess water was dried with a stream of nitrogen. For visualization, we used two platforms. We either plasma-bonded 500 µm wide, 90 µm deep polydimethylsiloxane (PDMS) microchannels fabricated using standard photolithography methods, or we deposited PDMS gaskets on the clean coverslips. PDMS gaskets were obtained using biopsy punches of 3 or 6 mm in diameter.

Sample preparation

Single colonies of the bacterial strains of interest were grown at 37°C in LB medium overnight. The culture was diluted 1:500 and grown to early-exponential phase before visualization. For motility visualization, cells in early-exponential phase were plated on plain LB-agar plates for 4 hours, harvested by gently flushing them with LB medium followed by a dilution to OD 600 < 0.05. The cells were loaded either into a microfluidic chip or in PDMS gaskets. Microfluidic chips were first loaded with plain LB medium. After proper tubing, exhaust tubes were dipped in bacterial culture and cells were loaded by aspiration using a syringe pump (Crpump, ZS100). The gasket were loaded with 20 µl of bacterial culture at OD 600 < 0.05, washing twice with fresh LB after 5 - 10 min of incubation at RT (if higher OD was used). After loading process was complete, gaskets were sealed with a small coverslip in order to prevent liquid evaporation that generated fluctuations on the iSCAT images.

We found that fliC cells had more TFP compared to WT. We attribute this difference to our sample preparation process which first selects for cells that reach and remain on the surface. This loading process induces a selection for more piliated cells that attach more strongly to the coverslip.

Experimental setup

Our experimental setup is adapted from Ortega *et al.* to allow live cell visualization during long acquisition times (see schematic in **Supplementary Figure 1**)[4]. We sought to reduce phototoxicity by using a laser wavelength of 635nm for the iSCAT channel (Lasertack, LDM-638-700-C). The illumination beam was spatially filtered through a 50 µm pinhole and collimated with a 4*f* lens. The collimated beam was aligned into two perpendicular acousto-optic deflectors (AODs), (AA Opto-Electronic, DTSXY-400-660) and imaged into the back focal plane of the objective (Olympus, PLAN APO 60x 1.42) thanks to a 4*f* lens system, a polarizing beam splitter (PBS) (Thorlabs, PBS251) and a quarter-wave plate (QWP) (Thorlabs, AQWP05M-600). The AODs allowed in-plane scanning of the beam on the sample. The objective captured the light scattered by the sample and the reflection of the incident beam at the glass-water interface. QWP and PBS discriminated input illumination from the reflected and scattered light. A 1000 mm focal length achromatic lens imaged the back focal plane of the objective onto a CMOS camera (PhotonFocus, MV1-D1024E-160-CL), yielding a 31.8 nm pixel size. Images were acquired using LabView and a frame grabber (National Instruments, PCIe-1433). We added a mechanical shutter into the illumination path to prevent unnecessary illumination. We also implemented a bright field channel by adding a white LED (Thorlabs, WFA1010) above the stage and imaged the back focal plane of the objective on a CMOS camera (PointGrey, CM3-U3-31S4M) with a 400 mm focal length achromatic lens (pixel size of 25.9 nm). This brightfield channel allowed localization of the cells before iSCAT acquisition thus protecting the cells against extended light exposure.

Autofocus system

We ensured the z-position stability of our sample by building a cytocompatible autofocus system with a weak infrared laser (850nm, 3,5mW) (Thorlabs, CPS850). A CMOS camera (Thorlabs, DCC1545M) detected the infrared light totally reflected by the glass-water interface and a LabView

software computed the correction of the drift providing real-time adjustment of the z-position of the stage through a piezo actuator.

Twitching motility assays

Motility assays were performed by stabbing and pipetting a 0.5% agarose LB plate with 2 µl of stationary phase *P. aeruginosa* culture at the gel-plastic interface. These plates were incubated 24 h at 30°C before removing agarose and staining the plastic dish with a 0.1% solution of crystal violet in water. We performed microscopic twitching visualizations (**Supplementary video 8**) by pipetting 0.5 µl of exponentially growing cells (OD = 0.1 at 600 nm) on a 0.5% agarose LB pad. These were then flipped onto a glass bottom dish (Mattek, #1.5 coverslip) and incubate at 30°C for 5 h. The leading edge of the expanding colonies were then visualized for 2 min at 1 fps by phase contrast microscopy on Nikon TiE equipped with a 100x, NA 1.45 objective and a Hamamatsu Orca R2 camera.

Image processing

To reveal the interferometric component of the signal, each frame of a given sequence was divided by a reference. This reference image was generated by computing the median of each pixel value throughout the whole stack of images. To improve visualization, we applied a band pass filter dampening the contributions of small and large structures (smaller than 1 pixel and larger than 13 pixel) with the FFT plugin of ImageJ[33]. To reduce slight temporal variation in illumination, each frame was divided by its mean pixel grey value.

Image analysis of pili dynamics quantification

In order to extract time delays between attachment and retraction to a tensed state we manually recorded the frame number of the pili tip attachment (appearing of a stationary dark spot at the pili tip) and the frame number of the pili under tension and without fluctuations from the pili were these events were clearly visible and measured with accuracy. Time delays were obtained by multiplying the frame difference by the acquisition frame time (frame rate: 200 fps). We measured tension times in 20 WT cells (27 retractions), 23 *fliC*$^{-}$ cells (54 events) and 30 *pilU*$^{-}$ *fliC*$^{-}$ cells (47 events) from data

acquired from at least 3 different days. Similarly, dwell times were obtained by manually measuring the time difference between attachment and detachment of each pilus from the same cells with the addition of 14 *pilT*$^{-}$ *fliC*$^{-}$ cells (45 events). Intensity measurements of attachment, tension and detachment were manually extracted by plotting the intensity profile along the pili using the ImageJ "plot profile" built-in tool. We performed intensity peak detections from the recorded profile for tip attachment and tension using MatLab (**Fig. 2** and **4**). Pili lengths were measured from pili tip attachment point to the middle of the first fringe of the cell body diffraction pattern from the same data set. (**Fig. 1** and **3**). Retraction frequencies were computed by counting all the obvious pili retractions within a movie but discarding the pili already tensed in the initial frames. The total number of retractions were then divided by the movie time for 30 *fliC*$^{-}$ and 23 *pilU*$^{-}$ *fliC*$^{-}$ cells (**Fig. 3**) from at least 3 biological replicates. Pili were counted on 20 WT, 15 *fliC*$^{-}$, 18 *fliC*$^{-}$ complemented, 19 *pilA*$^{-}$, 22 *pilA*$^{-}$ complemented, 11 *pilT*$^{-}$ *fliC*$^{-}$, 15 *pilT*$^{-}$ *fliC*$^{-}$ complemented, 18 *pilU*$^{-}$ *fliC*$^{-}$, and 17 *pilU*$^{-}$ *fliC*$^{-}$ complemented cells (**Fig. 1** and **3**) from the same strain culture. Flagella were counted from 52 WT, 51 *fliC*$^{-}$ and 50 *fliC*$^{-}$ complemented cells (**Supplementary Figure 2**) from at least 3 biological replicates.

Image analysis of cell motility with iSCAT

Cell motility movies were acquired at 10 fps and binned 10 times to obtain a final movie rate of 1 fps. Cell leading pole, defined as the center of the white spot in the middle of the circular fringes of the cell body, was manually tracked along the cell displacement (**Supplementary Figure 3**). Only cell displacements were no change in contrast of the leading pole was observed were recorded in order to assess effective influence of pili retraction to displacement and discard Brownian motion effects when the cell was not in contact with the glass surface. We note that some cells appeared to "hover" on the surface by Brownian motion, using TFP to maintain proximity to the surface. We recorded the number of visible retraction along each track. In total 14 tracks were recorded for WT cells, 13 for *fliC*$^{-}$ and 15 for *pilU*$^{-}$ *fliC*$^{-}$ from the same strain culture (**Fig 3** and **Supplementary Figure 4**).

Statistical analysis

As the time delay and tension time data were not normally distributed, we chose the median as an indicator of the central tendency of the distribution. Statistical analysis were performed using the bootstrap method in MatLab to resample our data into 300 different groups and computing the median of the median of each group to obtain a more robust estimate of the population's behavior. We computed the 95% confidence interval by taking the highest and lowest values of the bootstrap median dataset after removing the top and bottom 2.5% of the data points. The same approach has been used to determine retraction frequencies, pili lengths and displacement per retraction. Pili numbers in complementation analysis were analyzed by taking the mean of the bootstrap medians and the bootstrap 95% confidence interval as stated previously. A difference between two groups is defined as statistically significant when their 95% confidence intervals don't overlap.

Correspondence:

Correspondence and requests for material should be addressed to Alexandre Persat: alexandre.persat@epfl.ch

Acknowledgements:

The authors would like to thank Joanna Andrecka for valuable discussions on iSCAT, Joanne Engel and Yuki Inclan for strains and plasmids, Zainebe Al-Mayyah for help with generating one mutant strain. LT and AP thank the Swiss National Foundation for funding this work through the Projects grant 31003A_169377 and the Gabriella Giorgi-Cavaglieri Foundation.

Author contributions: L.T. and A.P conceptualized the study and performed experiments and data analysis. L.T., A.F., and P.K. implemented and adapted the iSCAT microscope for live cell imaging. L.T., P.K and A.P. wrote the manuscript.

Competing interests: Authors declare no competing interests.

Data availability: All data are available from the corresponding author upon reasonable request.

Code availability: All codes are available from the corresponding author upon reasonable request.

314

Bibliography:

1. Gibiansky, M. L. *et al.* Bacteria Use Type IV Pili to Walk Upright and Detach from Surfaces. *Science* **330**, 197–197 (2010).

2. Mattick, J. S. Type IV Pili and Twitching Motility. *Annu. Rev. Microbiol.* **56**, 289–314 (2002).

3. Chang, Y. W. *et al.* Architecture of the type IVa pilus machine. *Science* **351**, (2016).

4. Ortega Arroyo, J., Cole, D. & Kukura, P. Interferometric scattering microscopy and its combination with single-molecule fluorescence imaging. *Nat. Protoc.* **11**, 617–633 (2016).

5. Costa, T. R. D. *et al.* Secretion systems in Gram-negative bacteria: structural and mechanistic insights. *Nat. Rev. Microbiol.* **13**, 343 (2015).

6. Persat, A. Bacterial mechanotransduction. *Curr. Opin. Microbiol.* **36**, 1–6 (2017).

7. Burrows, L. L. Pseudomonas aeruginosa Twitching Motility: Type IV Pili in Action. *Annu. Rev. Microbiol.* **66**, 493–520 (2012).

8. Persat, A., Inclan, Y. F., Engel, J. N., Stone, H. A. & Gitai, Z. Type IV pili mechanochemically regulate virulence factors in Pseudomonas aeruginosa. *Proc. Natl. Acad. Sci. U. S. A.* **112**, 7563–7568 (2015).

9. Merz, A. J., So, M. & Sheetz, M. P. Pilus retraction powers bacterial twitching motility. *Nature* **407**, 98–102 (2000).

10. Maier, B., Potter, L., So, M., Seifert, H. S. & Sheetz, M. P. Single pilus motor forces exceed 100 pN. *Proc. Natl. Acad. Sci.* **99**, 16012–16017 (2002).

11. Beaussart, A. *et al.* Nanoscale Adhesion Forces of Pseudomonas aeruginosa Type IV Pili. *ACS Nano* **8**, 10723–10733 (2014).

12. Jin, F., Conrad, J. C., Gibiansky, M. L. & Wong, G. C. L. Bacteria use type-IV pili to slingshot on surfaces. *Proc. Natl. Acad. Sci.* **108**, 12617–12622 (2011).

13. Skerker, J. M. & Berg, H. C. Direct observation of extension and retraction of type IV pili. *Proc. Natl. Acad. Sci. U. S. A.* **98**, 6901–4 (2001).

14. Ellison, C. K. *et al.* Obstruction of pilus retraction stimulates bacterial surface sensing. *Science* **358**, 535–538 (2017).

15. Ortega Arroyo, J. *et al.* Label-free, all-optical detection, imaging, and tracking of a single protein. *Nano Lett.* **14**, 2065–2070 (2014).

16. Kukura, P. *et al.* High-speed nanoscopic tracking of the position and orientation of a single virus. *Nat. Methods* **6**, 923–927 (2009).

17. Ping, L., Birkenbeil, J. & Monajembashi, S. Swimming behavior of the monotrichous bacterium Pseudomonas fluorescens SBW25. *FEMS Microbiol. Ecol.* **86**, 36–44 (2013).

18. Ortega-Arroyo, J. & Kukura, P. Interferometric scattering microscopy (iSCAT): new frontiers in ultrafast and ultrasensitive optical microscopy. *Phys. Chem. Chem. Phys.* **14**, 15625 (2012).

19. Krishnan, M., Mojarad, N., Kukura, P. & Sandoghdar, V. Geometry-induced electrostatic trapping of nanometric objects in a fluid. *Nature* **467**, 692–695 (2010).

20. Bertrand, J. J., West, J. T. & Engel, J. N. Genetic analysis of the regulation of type IV pilus function by the Chp chemosensory system of Pseudomonas aeruginosa. *J. Bacteriol.* **192**, 994–1010 (2010).

21. Whitchurch, C. B. & Mattick, J. S. Characterization of a gene, pilU, required for twitching motility but not phage sensitivity in Pseudomonas aeruginosa. *Mol. Microbiol.* **13**, 1079–1091 (1994).

22. Park, H.-S. M., Wolfgang, M. & Koomey, M. Modification of Type IV Pilus-Associated Epithelial Cell Adherence and Multicellular Behavior by the PilU Protein of Neisseria gonorrhoeae. *Infect. Immun.* **70**, 3891–3903 (2002).

23. Kuchma, S. L. *et al.* Cyclic Di-GMP-Mediated Repression of Swarming Motility by Pseudomonas aeruginosa PA14 Requires the MotAB Stator. *J. Bacteriol.* **197**, 420–430 (2015).

24. Chiang, P., Habash, M. & Burrows, L. L. Disparate Subcellular Localization Patterns of Pseudomonas aeruginosa Type IV Pilus ATPases Involved in Twitching Motility. *J. Bacteriol.* **187**, 829–839 (2005).

25. Giltner, C. L., Nguyen, Y. & Burrows, L. L. Type IV pilin proteins: versatile molecular modules. *Microbiol. Mol. Biol. Rev. MMBR* **76**, 740–72 (2012).

26. Thomas, W. E., Vogel, V. & Sokurenko, E. Biophysics of Catch Bonds. *Annu. Rev. Biophys.* **37**, 399–416 (2008).

27. Biais, N., Higashi, D. L., Brujic, J., So, M. & Sheetz, M. P. Force-dependent polymorphism in type IV pili reveals hidden epitopes. *Proc. Natl. Acad. Sci. U. S. A.* **107**, 11358–11363 (2010).

28. Kiehn, O. Decoding the organization of spinal circuits that control locomotion. *Nat. Rev. Neurosci.* **17**, 224–238 (2016).

29. Dietz, V. Proprioception and locomotor disorders. *Nat. Rev. Neurosci.* **3**, 781–790 (2002).

30. Persat, A. *et al.* The Mechanical World of Bacteria. *Cell* **161**, 988–997 (2015).

31. Hmelo, L. R. *et al.* Precision-engineering the Pseudomonas aeruginosa genome with two-step allelic exchange. *Nat. Protoc.* **10**, (2015).

32. Young, G. *et al.* Quantitative mass imaging of single biological macromolecules. *Science* **360**, 423–427 (2018).

33. Schindelin, J. *et al.* Fiji: an open-source platform for biological-image analysis. *Nat. Methods* **9**, 676–682 (2012).

383

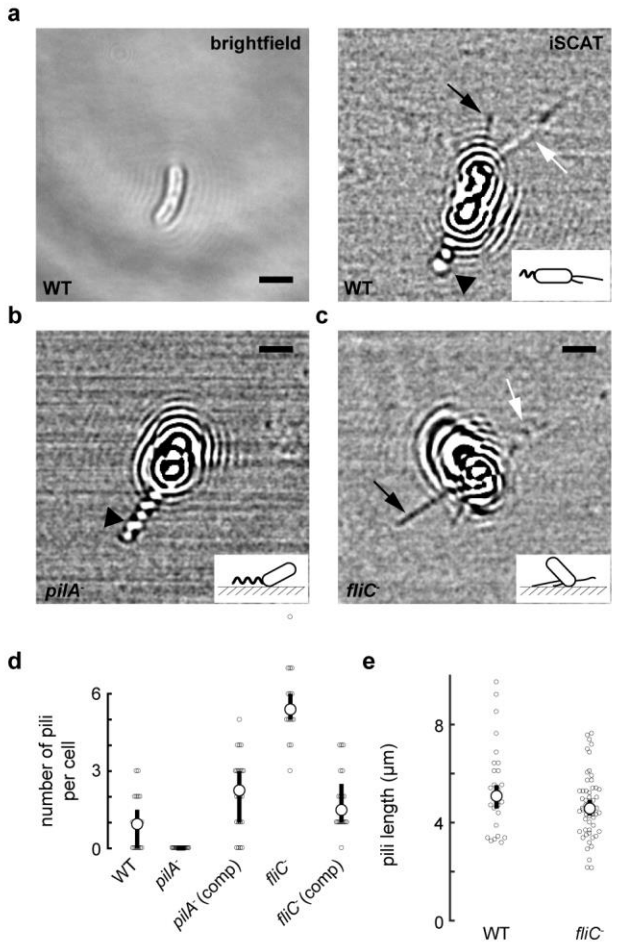

Fig. 1. iSCAT reveals extracellular bacterial filaments. (a) Brightfield (left) and iSCAT (right) images of a single WT *P. aeruginosa* cell. The brightfield image only shows the rod-shaped body of the bacterium, while multiple extracellular structures are visible in iSCAT. Flagellum (black arrowhead) and type IV pili with constant (black arrow) or spatially varying contrast (white arrow). (b) A deletion mutant of the pilin gene *pilA* displayed no extracellular slender structures, while (c) a mutant in the flagellin subunit gene *fliC* had no polar filaments with alternating contrast. Inserted illustrations in iSCAT images show the position of cell and filaments relative to the coverslip surface. (d) Quantification of mean TFP per cell with iSCAT. WT has about one pilus per cell in average, (number of cells from the same culture n = 20), *pilA*$^-$ has none (n = 19) but WT levels are restored in the complemented strain (n = 22). *fliC*$^-$ mutant cells have more TFP than WT (n = 15), which decreases to WT level in the complemented strain (n = 18). We attribute the hyperpiliation of *fliC*$^-$ to a selection effect during sample loading (see Materials and Methods). Small circles are individual

measurements, large circles are means of bootstrap medians, error bars represent bootstrap 95% confidence interval. (e) Attached TFP length distribution in WT (combined number of pili from cells imaged in at least three biological replicates $n = 27$) and *fliC*$^{-}$ ($n = 54$). The flagellum-less mutant has no defect in TFP length. Small circles represent individual measurements, large circles are bootstrap medians and error bars bootstrap 95% confidence interval. (a, b, c) Scale bars: 2 µm.

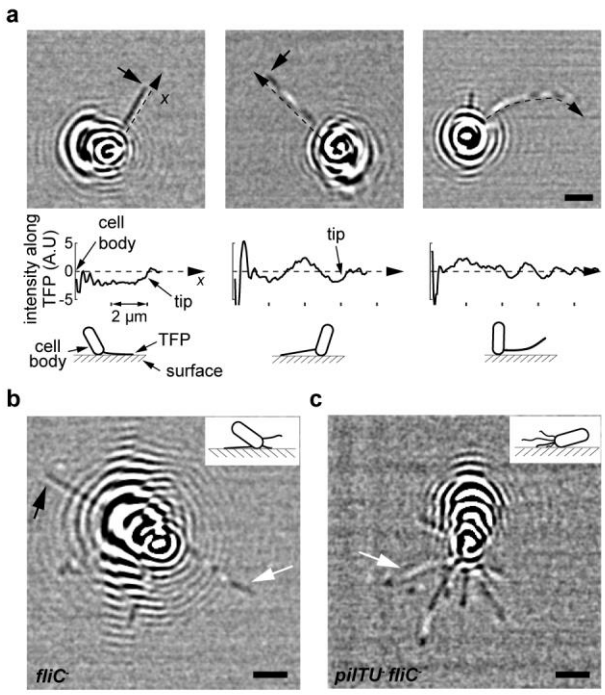

Fig. 2. Visualization of TFP position and retraction in three dimensions. (a) Images of three representative TFP positions and orientations visualized by iSCAT, with corresponding iSCAT intensity values along the length of the fiber (below). Changes in iSCAT contrast allows us to infer pilus position in 3D. TFP that have constant contrast are flat on the surface (left panel), the ones with alternating contrast form a finite angle with the coverslip (middle panel), and curved fibers with oscillating and irregular contrast are defined as “floppy” (right panel). Below each image, a plot of the pixel grey value along the pilus allows us to determine if the pili lay flat, at an angle or are fluctuating. The illustration represents the putative 3D orientation of the pilus and the cell body. (b) TFP of *fliC*$^{-}$ deletion mutant cells exhibit all three morphologies (**Supplementary video 3)**. (c) Cells lacking both retraction motor genes *pilT* and *pilU* only show floppy TFP, demonstrating retraction and tension force generates straight TFP morphology (**Supplementary video 4)**. We encountered these features throughout all our visualizations. Tensed, flat or at an angle, and floppy pili were observed with similar results in all our retractile strains (WT, *fliC*$^{-}$, and *pilU*$^{-}$ *fliC*$^{-}$). Whereas only the floppy pili were observed in our *pilT*$^{-}$ *fliC*$^{-}$. (a, b, c) Scale bars: 2 µm.

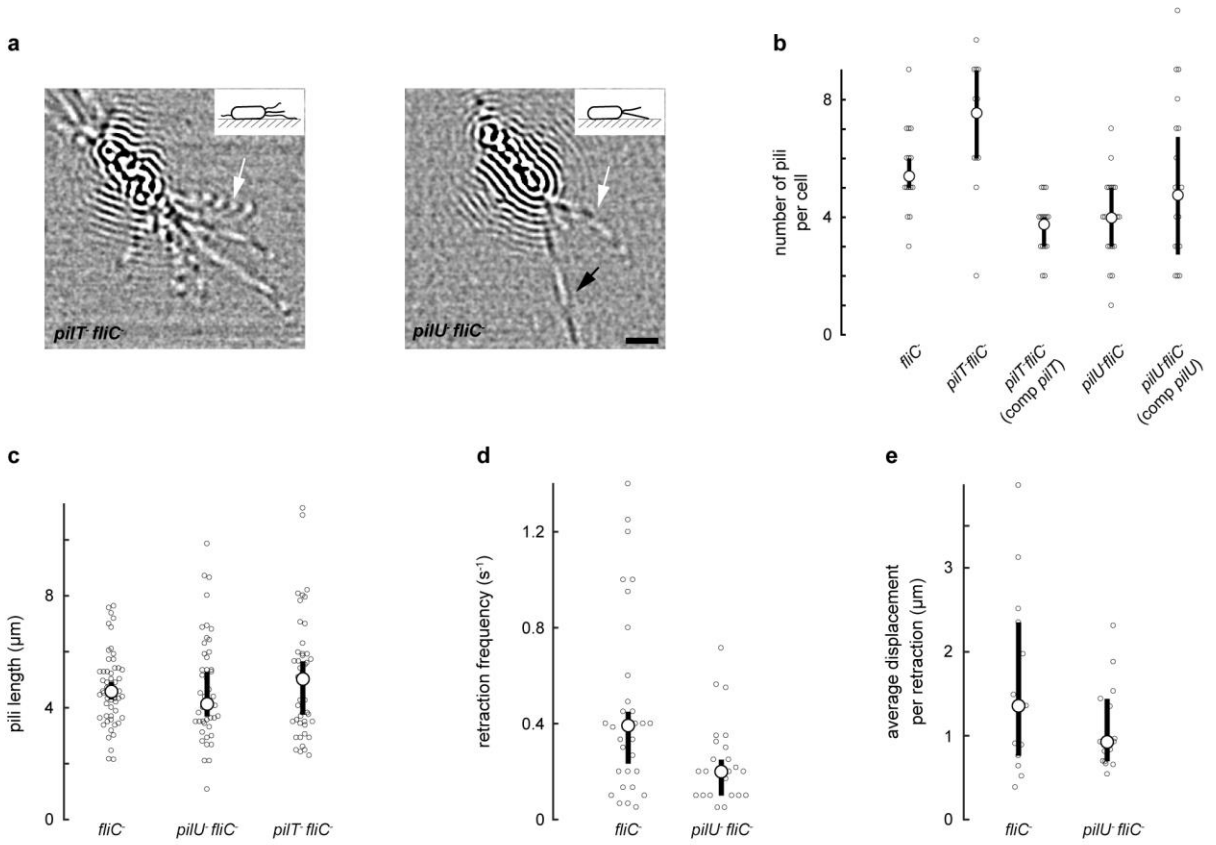

418

419 **Fig. 3. PilU does not affect TFP dynamics in free solution.** (a) iSCAT images of *pilT⁻ fliC⁻* and
420 *pilU⁻ fliC⁻* mutants. *pilT⁻ fliC⁻* cells never undergo retraction on the timescale of our movies. The *pilU⁻*
421 *fliC⁻* mutant picture shows a retraction of one TFP. Scale bar: 2 µm. (b) Number of TFP in motor
422 mutants and their corresponding complementation strains. These have similar numbers of surface
423 pili except *pilT⁻ fliC⁻* (number of cells from the same culture *n* = 11), which had more (*fliC⁻ n* = 15,
424 *pilT⁻ fliC⁻* complemented *n* = 15, *pilU⁻ fliC⁻ n* = 18, *pilU⁻ fliC⁻* complemented *n* = 17). Large circles are
425 means of bootstrap medians and error bars bootstrap 95% confidence intervals. Small circles are
426 individual measurements. (c) The average lengths of TFP that attached on the glass surface in *fliC⁻*
427 (combined number of pili from cells imaged in at least three biological replicates *n* = 54), *pilU⁻ fliC⁻* (*n*
428 = 47) and *pilT⁻ fliC⁻* (*n* = 45). (d) Retraction frequencies for *pilU⁻* mutant (combined number of pili
429 from cells imaged in at least three biological replicates *n* = 23,) compared to *fliC⁻* (*n* = 23). The *pilU⁻*
430 mutant show a slight decrease in retraction frequencies compared to *fliC⁻*. (e) Average displacement
431 per retraction for *fliC⁻* (number of tracks *n* = 13) and *pilU⁻ fliC⁻* (*n* = 15). Motility does not strongly

differ between these mutans. (c,d,e) Small circles correspond to individual measurements, large circles are medians of bootstrap medians and error bars are bootstrap 95% confidence interval. A difference between two groups is defined as statistically significant when their 95% confidence intervals don’t overlap.

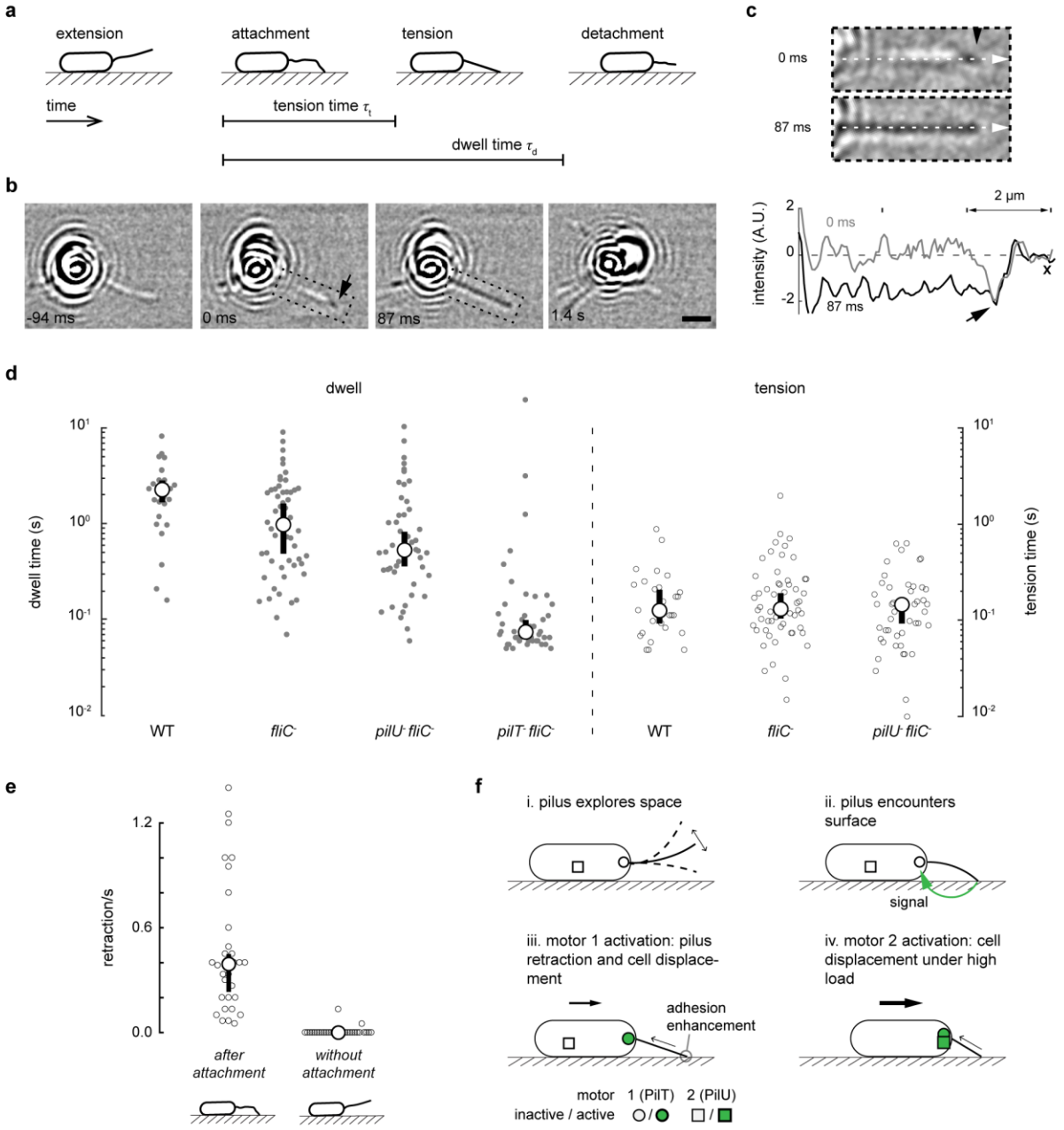

Fig. 4. Coordination of TFP retraction motors. (a) Illustration of the optimal sequence of events for TFP function: extension, attachment, tension and release from the surface. (b) Successive events from (a) visualized with iSCAT. Attached pilus tip appears as a stationary dark signal at 0 ms (black arrow). The whole fiber transitions into lower intensity values at τ_t = 87 ms, before detaching at τ_d = 1.4 s. Scale bar: 2 µm (c) Close up view of attachment and tension from (b) with corresponding intensity profile along the pilus. A dip in intensity is observed at the tip at 0 ms (black arrow on image and graph), transitioning to a uniform low value at τ_t. (d) Measurements of dwell and

tension times in WT (total number of pili from at least three biological replicates n = 27), *fliC*$^-$ (n = 54) and *pilU*$^-$ *fliC*$^-$ (n = 47) and *pilT*$^-$ *fliC*$^-$ (n = 45). Comparing retraction-capable to retraction-deficient mutants show that TFP tension increases dwell time. The tension times in the retraction-capable cells are close to the dwell time of *pilT*$^-$ *fliC*$^-$, showing that motors engage rapidly to initiate retraction. There is no defect in tension time in *pilU*$^-$ *fliC*$^-$ indicating that PilT is sufficient to initiate this rapid response. (e) TFP retraction frequencies for attached and unattached TFP in *fliC*$^-$ (number of cells from at least three biological replicates n = 30). TFP retract almost only after their tips touch the surface, indicating attachment stimulates retraction. (d and e) Small circles correspond to individual measurements, large circles to median and error bars to bootstrap 95% confidence intervals. A difference between two groups is defined as statistically significant when their 95% confidence intervals don't overlap. (f) Proposed model for sequential control of TFP motion. During spatial fluctuations (i), attachment of TFP tip to the surface generates a signal activating PilT (ii). This causes pilus retraction and tension, reinforcing attachment and resulting in longer dwell times and cell displacement (iii). PilU engages to power cell displacement under strong loads, for example in environments with increased friction on the cell body (iv).